2020 IEEE 61st International Scientific Conference on Power and Electrical Engineering of Riga Technical University (RTUCON)

Induction Machine HiL Setup Implementation and IFOC Testing Based on the OP4510 Realtime Computer

Matiss Stunda[a,b,c*], Mohamed El Baghdadi[b,c], Leonids Ribickis[a], Omar Hegazy[b,c]
[a]Riga Technical University, Faculty of Electrical and Environmental Engineering,
Institute of Industrial Electronics and Electrical Engineering, Riga, Latvia
[b]Vrije Universiteit Brussel (VUB), ETEC Department & MOBI Research Group, Pleinlaan 2,1050 Brussels, Belgium
[c]Flanders Make, 3001 Heverlee, Belgium
*Corresponing author: matiss.stunda@rtu.lv

***Abstract*—This work discusses the practical development of a HiL induction machine test rig. An OP4510 realtime computer by Opal-RT is used to run the vector control algorithm designed in Matlab Simulink. Assembly and configuration of the setup are outlined. Initial test results of IFOC in torque control mode are discussed. Effects of d-q cross coupling due to motor parameter inaccuracies are demonstrated.**

***Index Terms*—Field Oriented Control; Electric Traction Drive; Hardware in the Loop; Induction Machine Vector Control; Opal-RT; Matlab Simulink**

Introduction

The development of induction motor drives has seen both steady incremental progress as well as several major leaps in performance due to new concepts and technologies. Introduction of power semiconductor inverters in the mid-20th century introduced continuous and efficient modulation of the shaft speed. Decades later, the introduction of vector control strategies enabled accurate, responsive and more efficient performance of induction machine drives.

Today, along with the evolution of available embedded processing hardware, increasingly advanced electrical drive control concepts can be evaluated - both novel ones as well as old but previously unfeasible ones.

The theoretical research of a control algorithm can be first done by modelling the whole system i.e. doing a Model in the Loop (MiL) simulation. This includes using a software model of the power inverter and electrical machine [1]. Further on, to obtain an absolutely realistic view of the control system's performance, a Hardware in the Loop (HiL) test must be done. In this setup physical power electronics and electrical machine hardware are connected to the simulated algorithm.

To investigate the control algorithm performance in a HiL test setup, both appropriate processing hardware and power electronics are required.

This paper discusses the assembly and configuration of a HiL test system based on an *Opal-RT* OP4510 realtime computer. The system operates with control algorithms designed in *MATLAB Simulink* modelling environment.

978-1-7281-9510-0/20/$31.00 ©2020 IEEE

In the first section, used hardware is described. The second section looks at the mathematical model and it's implementation requirements. In the last two sections the setup and results are described for testing the basic flux observer operation in different steady sate modes. By using initial motor parameter values, the general functionality of the OP4510 based Indirect Field-Oriented Control (IFOC) system is validated. Meanwhile the effects of motor model inaccuracies are demonstrated and discussed.

I. Hardware Setup

A. Main Drive

The main drive comprises the main machine and power inverter ("Inverter" in Fig. 1). It is controlled by the tested algorithm. In this case, the main or driving machine is an induction machine (IM) with the nominal power of 2.6 kW.

Interfacing a control algorithm with the electrical machine requires a power inverter with safely and reliably operating power electronics stage as well as low-level access to the control stage. An approach often taken is using an industrial power inverter that is modified to provide direct access to power switch states. A *Danfoss* power inverter is used to drive the main machine. The given inverter is a modified version for research purposes. Instead of standard parametric control, direct access to inverter output states is provided. This allows the implementation of any algorithm in the finest timescale. Meanwhile, sufficient protective functionality is kept on the gate control module of the inverter. This includes dead-time management to prevent shoot-through states of the power transistors. Overcurrent and overvoltage trip is also integrated to protect the power electronics from damage. The industrially designed power stage provides stable and electromagnetically solid operation.

The inverter is connected to the realtime computer through five optical fiber channels.

First channel is an active-high "enable" channel that puts the inverter bridge in a free-wheeling state when disabled. This disabled state is equivalent to the trip state in case of overload or fault detection.

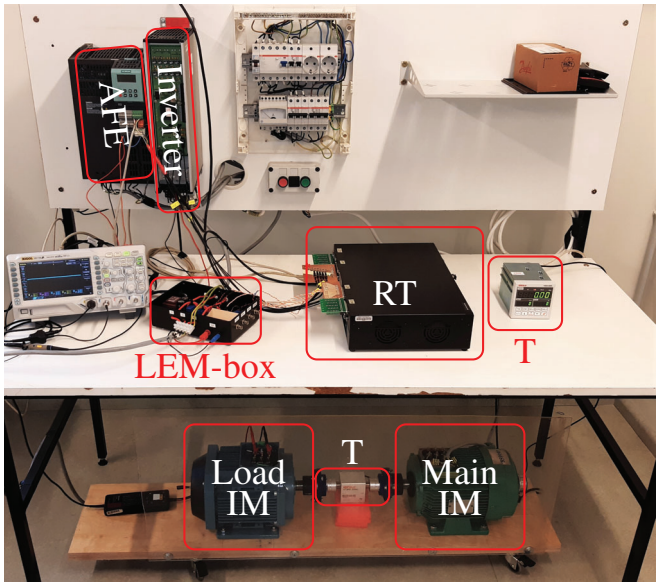

Fig. 1: Motor test rig setup; T - torque meter; RT - OP4510; AFE - bidirectional load inverter

Three input channels provide control over the inverter output phases. As mentioned, the dead-time control is integrated in the inverter control card. This generates three pairs of complementary PWM gate control signals for the upper and lower transistors.

Lastly a "chopper" channel controls the power switch of a DC-bus discharge resistor. The discharge resistor can be used to provide an energy outlet in case the main machine is driven into generator mode by the load drive.

An adaptor card was produced to couple the five optic-fiber channels to the DB-37 digital-output connector of the OP4510.

B. Load Drive

The load machine is in this case an induction machine of rated power of 3.5kW. Having a higher power rating than the main machine makes it possible to enforce the full torque and power range on the driving machine.

The load machine is driven by an Active Front-End (AFE) inverter with an active (bidirectional) rectifier bridge. This allows the power drawn by the main machine to be mostly returned to the grid. The AFE is also an industrial product from *Siemens*. It can be controlled by digital and analog control inputs.

C. Realtime computer

To run a HiL system the control algorithm needs to be executed in realtime as it is connected to the physical drive. For this purpose the Matlab-Simulink system is divided in two domains - realtime (SM_Master) and user interface (SC_Control). The realtime section is compiled to binary files and loaded onto the OP4510, where it runs with a sample time of $T_s = 50\mu s$. The user interface part is run on a personal computer (PC) as a Matlab-Simulink simulation with limited update frequency.

All the calculations required for the algorithm to operate are located and performed in the realtime section. This is the central part of the system as it faces two directions - the user PC and the physical system. The PC is connected by an Ethernet cable through which user commands are sent and process values received for monitoring. The physical system is connected through analog an digital inputs and outputs using DB37 connectors.

D. Control and feedback circuits

The analog and digital controls of the load drive may be setup according to the required load profile. For process control, no feedback is essential from the load drive to the OP4510 as the load drive has its own control loop. However, an analog signal is read from the torque transducer for monitoring and analysing the loaded tests.

The analog and digital inputs and outputs of the OP4510 are written and read once every program sample time T_s.

To modulate the main drive voltage, digital outputs in high resolution PWM mode are used. The frequency of three center-aligned PWM channels is set to 10 kHz. The new calculated duty cycles are set once per T_s.

To test an advanced control system against a conventional vector control system, five feedback signals are implemented: DC bus voltage u_{DC}, three phase currents i_a, i_b, i_c and rotor shaft speed ω_r.

Technically performance can be enhanced by also adding phase voltage measurements. In Direct Torque Control (DTC) this can improve precision of the voltage integrator by excluding transistor voltage drop. Speed sensorless control algorithms may also require phase voltage measurements to avoid errors due to voltage drops, especially at low speeds [2].

However, in production drives phase voltage measurement is usually not economically feasible [3]. The given set of five transducers should therefore suffice in an advanced system for it to be commercially competitive.

The voltage and current measurements are done by *LEM* isolated Hall-effect current transducers ("LEM-box" in Fig. 1).

For the shaft speed an incremental pulse encoder is sufficient as the rotor of an induction machine is symmetrical and it's exact position does not matter unless position control is desired.

To read the encoder signal, digital inputs of the OP4510 are used in high resolution event detection mode. In this mode, after each sampling period T_s an array of time values is updated for each channel. These represent the times of encoder pulse edges detected during the sampling period T_s.

Depending on w_r, one sampling period can see either a single or multiple edges on one or both encoder quadrature channels "A" and "B". A function block was created to analyze the detected pulse edges and calculate w_r. This selects among the available events ones that are the furthest apart in order to maximize the precision.

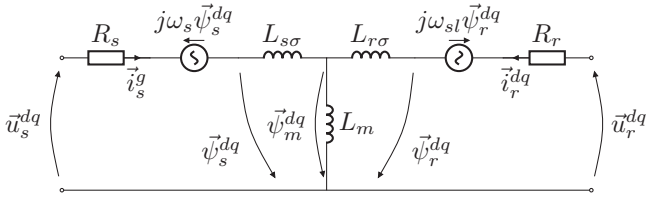

Fig. 2: Equivalent circuit of the induction machine in the synchronous reference frame [3]

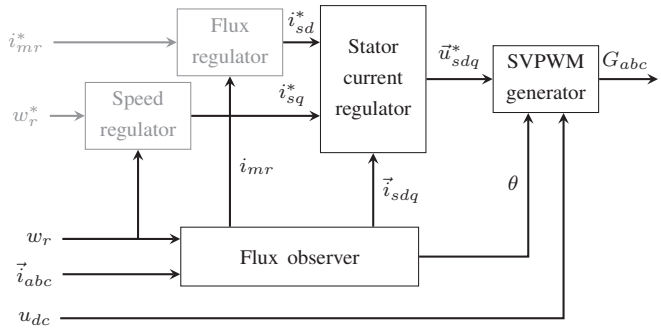

Fig. 3: The structure of a conventional FOC algorithm

II. Control model

As a general case, the test setup will be validated for the sensored Indirect Field Oriented Control (IFOC) strategy. IFOC is among the most basic vector-control approaches used for three phase induction machine control. The general IFOC principle is shown in Fig. 3.

Most of advanced motor control techniques rely on measuring or estimating the position of some magnetic flux linkage vector [4]. This is then used to efficiently adjust the relative position of the output voltage control reference.

The core concept of IFOC is to estimate the slip frequency ω_{sl} by measuring stator currents. To estimate ω_{sl}, the induction motor equivalent model in the direct-quadrature (d-q) reference frame (Fig. 2.) is used. The d-q reference frame is a Cartesian plane with d-axis as the abscissa and q-axis as the ordinate. The d-axis must in principle be aligned with the rotor flux linkage vector $\vec{\psi}_r$. Therefore the d-q frame rotates at the synchornous frequency ω_s.

In the following discussion, $\vec{i}_{sdq} = i_{sd} + ji_{sq}$ is considered a vector in the d-q reference frame. It is composed of direct current i_{sd} and quadrature current i_{sq}.

The list of equations describing the IM model were reiterated in [5]. On the premise that the rotor equivalent resistance R_r and rotor equivalent inductance L_r are known, a simple calculation of ω_{sl} can be derived from the set of equations [6].

The estimated ω_{sl} is used to determine the rotor flux linkage vector $\vec{\psi}_r$ position and align the d-q reference frame with it. If the d-q reference frame is aligned successfully, dynamic and proportional torque control can be achieved by modulating the q-axis component of the stator current i_{sq}. If the reference frame is not well-aligned with $\vec{\psi}_r$, cross-coupling occurs and responsiveness to control inputs is reduced. This happens because part of the control reference is directed towards the damped process of rotor magnetization [3].

As is demonstrated by [6], ω_{sl} can be expressed as a function of only i_{sd}, i_{sq} and the value of R_r/L_r. Of course, in practice, accurate knowledge of R_r and L_r is problematic as the parameters tend to change under operation. The calculation of R_r and L_r also depends on the other model parameters which undergo variation as well.

The problem of motor parameter identification has seen numerous different approaches. The parameters can be calculated by nameplate data [7] or different physical tests before operation [8]. Methods for updating the values during operation include pre-calculated adjustment curves, intrusive online measurements [9] as well as non-intrusive model based parameter observer algorithms [10].

For the initial testing an approximate value of $R_r/L_r = 5.16$ was selected based on automatic identification tests performed with the load drive AFE inverter.

III. Simulink interface setup

For gradual verification and troubleshooting of the system, a flexible control panel was constructed with the possibility to switch between different control methods. Access to motor parameters and voltage-current limits was also added.

First, to validate the inverse Park and SVPWM functionality, the open-loop v/f control method is used. The angle θ is generated by integrating the user set frequency. The reference voltage u^*_{sd} of the inverse Park tranform is adjusted linearly up to base speed where it reaches U_n set in the control panel. u^*_{sd} remains at zero as it is irrelevant in this mode. Above $f_n = 50Hz$, field weakening takes place as the value of $\psi_s \sim u_s/\omega_s$ starts to decrease. By decreasing U_n below the actual machine value, field weakening can be achieved within base speed.

In a second setup, current controlled operation is tested. Stator current commanded value $\vec{i}^*_{sdq}$ is set by the user (as d and q components). Actual stator current $\vec{i}_{sdq}$ is calculated by a Park transform block. The stator voltage $\vec{u}^*_{sdq}$ required to achieve $\vec{i}_{sdq} = \vec{i}^*_{sdq}$ is calculated by the d and q PI controllers and fed to an inverse Park transform block. The angle θ of both Park and inverse Park transforms is still dictated by user set frequency.

IFOC algorithm is implemented in the third step. For the tests covered in this paper, the IFOC is run in torque control mode. This eliminates the speed control loop. The flux regulator loop is also excluded to directly analyze the impact of i^*_{sd} and i^*_{sq} set by the user. The reduction of the control loop cascade is represented by the greyed out blocks in Fig. 3.

IV. IFOC strategy verification

A. Reference and measurements

For torque control testing the load drive was set up at speed controlled mode and maintains the shaft speed at 1500 RPM, which corresponds to the nominal synchronous speed. Different $\vec{i}^*_{sdq}$ references are passed to the controller and the voltage

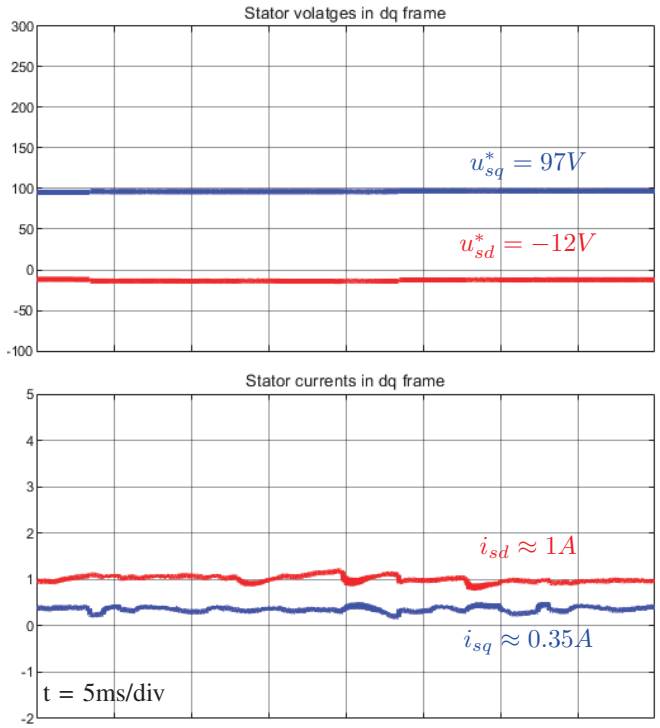

Fig. 4: Scope view $\vec{u}^*_s$ and $\vec{i}_s$ in dq reference frame; $T_m = 0Nm$, $i^*_d = 1A$, $i^*_q = 0.35A$

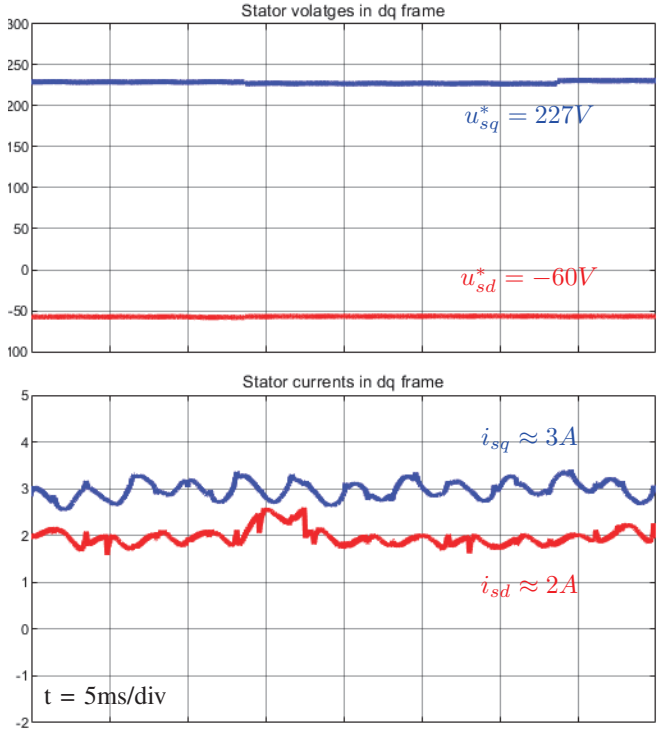

Fig. 5: Scope view $\vec{u}^*_s$ and $\vec{i}_s$ in dq reference frame; $T_m = 4.62Nm$, $i^*_d = 2A$, $i^*_q = 3A$

reference is observed $\vec{u}^*_{sdq}$ in the Simulink scope. This is the voltage required to achieve the current reference $\vec{i}^*_{sdq}$. The scope view is shown in Fig. 4 and Fig. 5. Actual achieved $\vec{i}_{sdq}$ values are also visible.

It is important to note that the actual $\vec{i}_{sdq}$ value matches $\vec{i}^*_{sdq}$ in average value but has an substantial fluctuating component proportional to the load. This is a result of DC-bus voltage distortion caused by the fluctuating DC-bus current.

This is represented by the difference in current shape between Fig. 4 and Fig. 5. A higher current magnitude results in higher DC-link distortion. Six fluctuations per 20ms correspond to the current shape drawn from the DC link capacitor by a three-phase inverter driving a 4 pole electrical machine around 1500 RPM.

This indicates the importance of compensation mechanisms for elimination of voltage regulator sensitivity to DC-bus voltage fluctuations [11].

Seven different $\vec{i}^*_{sdq}$ references are passed to the controller. These are plotted on the d-q reference frame in Fig. 6. The mechanical torque value T_m resulting from each commanded $\vec{i}^*_{sdq}$ vector is noted next to it.

The torque is assumed positive in the direction of shaft rotation. Thereby the main drive "attempts" to accelerate the load.

B. Test results

First, it is attempted to magnetize the main machine without applying torque on the shaft.

In the IFOC setup, θ is generated by the flux observer. Under correct flux observer operation, with i^*_{sq} set to zero θ should be synchronous to the shaft speed enforced externally by the load, i.e. no torque should be exerted.

To magnetize the machine i^*_{sd} was set to $1A$. At this point it was observed that the resulting torque value is not zero. To achieve zero torque, the current reference $\vec{i}^*_{sdq}$ needed to be shifted counterclockwise by increasing i^*_{sq} from $0A$ to $0.35A$. The same effect was observed with $i^*_{sd} = 2A$. To achieve $T_m = 0Nm$, the required quadrature current was $i^*_{sq} = 0.47A$.

Given the placement of $\vec{i}^*_{sdq}$ at zero torque, the approximate direction of $\vec{\psi}_r$ is indicated by the dashed vector in Fig. 6. This indicates imprecision of the motor parameters the location of the d axis is the expected position of $\vec{\psi}_r$ incorrectly estimated by the flux observer. The cross-coupling effect is thereby introduced, which is seen in the further measurement results.

By leaving the i^*_{sd} value at $2A$ and increasing i^*_{sq} to $1A$, $2A$ and $3A$ the produced torque T_m should increase proportionally. However it is apparent that the gain $\Delta T_m/\Delta i_{sq}$ is not constant.

The values of $\Delta T_m/\Delta i_{sq}$ for the three steps $i_{s1} \rightarrow i_{s2}$, $i_{s2} \rightarrow i_{s3}$ and $i_{s3} \rightarrow i_{s4}$ are $1.45Nm/A$, $1.80Nm/A$ and $2.34Nm/A$ respectively.

Here the cross-coupling effect becomes evident as increase of i_{sq} in the misaligned d-q reference frame increases the $|\vec{\psi}_r|$ value as well.

Equation (1) expresses torque generation in terms of the $\vec{\psi}_r$ and $\vec{i}_s$ vectors [3]. The cross product dictates that T_m is

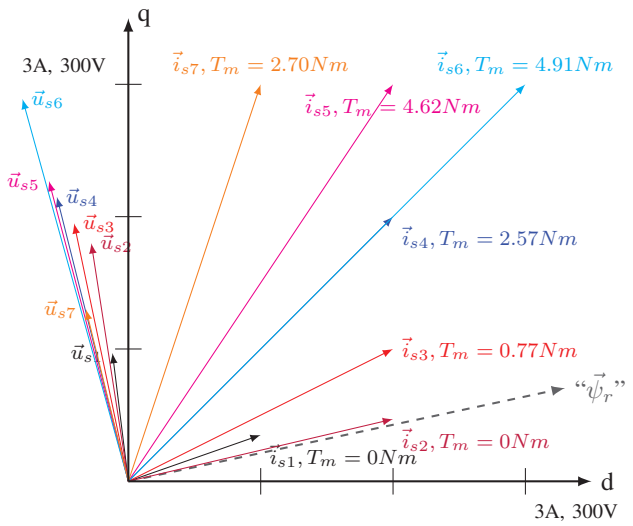

Fig. 6: Vector representation of $\vec{u}_s^*$ and $\vec{i}_s$

essentially proportional to $i_{sd} \cdot i_{sq}$ if the d-axis is aligned to $\vec{\psi}_r$.

$$\vec{T} = \frac{3}{2} p \frac{L_m}{L_r} \vec{\psi}_r \times \vec{i}_s \tag{1}$$

With the d-q frame misaligned, the actual torque value is proportional to the area between a given $\vec{i}_s$ vector and it's projection on the "$\vec{\psi}_r$" axis.

V. Conclusions

Basic operation of the IFOC algorithm was achieved in a HiL setup using the OP4510 realtime computer. By modulating i_{sd} and i_{sq} stator current components and analyzing the mechanical torque T_m, the cross coupling of the d-q terms was observed. This indicates the need for enhanced machine parameter estimation.

To improve the test setup performance a u_{dc} ripple compensation algorithm will be implemented in the next stage.

References

[1] M. Vafaeipour, M. El Baghdadi, F. Verbelen, P. Sergeant, J. Mierlo, and O. Hegazy, "Experimental implementation of power-split control strategies in a versatile hardware-in-the-loop laboratory test bench for hybrid electric vehicles equipped with electrical variable transmission," *Applied Sciences (Switzerland)*, vol. 10, no. 12, 2020.

[2] S. Lim, "Sensorless-FOC With Flux-Weakening and MTPA for IPMSM Motor Drives," Texas Instruments, Tech. Rep. SPRACF3, Apr. 2018. [Online]. Available: https://www.ti.com/lit/an/spracf3/spracf3.pdf

[3] J. Pyrhönen, V. Hrabovcová, and S. Semken, *Electrical Machine Drives Control: An Introduction*. John Wiley & Sons, Ltd, 2016.

[4] R. De Doncker, D. Pulle, and A. Veltman, *Advanced Electrical Drives: Analysis, Modeling, Control*, ser. Power Systems. Springer Netherlands, 2011.

[5] M. Stunda, "A space vector based tool for the visualisation of induction machine operation modes (accepted for publication)," in *2019 IEEE 60th International Scientific Conference on Power and Electrical Engineering of Riga Technical University (RTUCON)*, 2019.

[6] (2020) Induction Machine Flux Observer. MathWorks. [Online]. Available: https://se.mathworks.com/help/physmod/sps/ref/inductionmachinefluxobserver.html

[7] O. Avalos, E. Cuevas, and J. Gálvez, "Induction Motor Parameter Identification Using a Gravitational Search Algorithm," *Computers*, Apr. 2016.

[8] T. C. Chen, J. S. Chen, and C. C. Tsai, "Measurement of induction motor parameter identification," in *[1991] Conference Record. IEEE Instrumentation and Measurement Technology Conference*, 1991, pp. 288–291.

[9] M. Nomura, T. Ashikaga, M. Terashima, and T. Nakamura, "A high response induction motor control system with compensation for secondary resistance variation," in *1987 IEEE Power Electronics Specialists Conference*, 1987, pp. 46–51.

[10] S. Maiti, C. Chakraborty, Y. Hori, and M. C. Ta, "Model Reference Adaptive Controller-Based Rotor Resistance and Speed Estimation Techniques for Vector Controlled Induction Motor Drive Utilizing Reactive Power," *IEEE Transactions on Industrial Electronics*, vol. 55, no. 2, pp. 594–601, 2008.

[11] J. Su, R. Gao, and I. Husain, "Model Predictive Control Based Field-Weakening Strategy for Traction EV Used Induction Motor," *IEEE Transactions on Industry Applications*, vol. 54, no. 3, pp. 2295–2305, 2018.

This is a post-print of a paper published in Proceedings of the 2020 IEEE 61st International Scientific Conference on Power and Electrical Engineering of Riga Technical University (RTUCON 2020) and is subject to IEEE copyright.
https://doi.org/10.1109/RTUCON51174.2020.9316592
Electronic ISBN: 978-1-7281-9510-0.
USB ISBN: 978-1-7281-9509-4.
Print on Demand (PoD) ISBN: 978-1-7281-9511-7.